

Article

Modeling Parallel Robot Kinematics for 3T2R and 3T3R Tasks using Reciprocal Sets of Euler Angles

Moritz Schappler^{1,*}, Svenja Tappe¹ and Tobias Ortmaier¹

¹ Institut für Mechatronische Systeme, Leibniz Universität Hannover;
firstname.lastname@imes.uni-hannover.de

* Correspondence: moritz.schappler@imes.uni-hannover.de;

Abstract: Industrial manipulators and parallel robots are often used for tasks like drilling or milling, that require three translational, but only two rotational degrees of freedom (“3T2R”). While kinematic models for specific mechanisms for these tasks exist, a general kinematic model for parallel robots is still missing. This paper presents the definition of the rotational component of kinematic constraints equations for parallel robots based on two reciprocal sets of Euler angles for the end-effector orientation and the orientation residual. The method allows to completely remove the redundant coordinate in 3T2R tasks and to solve the inverse kinematics for general serial and parallel robots with the gradient-descent algorithm. The functional redundancy of robots with full mobility is exploited using nullspace projection.

Keywords: Parallel robot; five-DoF task; 3 T2R task; functional redundancy; task redundancy; redundancy resolution; reciprocal Euler angles; inverse kinematics

1. Introduction

Industrial tasks like welding, gluing, milling or drilling represent a major part of the applications of industrial robots, which generally have full mobility, i.e. the operational space of their end-effector has three translational and three rotational (“3T3R”) degrees of freedom (“DoF”). Parallel robots like the Stewart-platform have especially been proposed for milling tasks regarding their high structural stiffness. The task space of the named applications can be defined by three translational DoF and only two rotations due to a symmetry around the tool axis (“3T2R”). This results in a functional or task redundancy, which is not exploited to full extend yet for *parallel* robots.

1.1. Inverse Kinematics and Resolution of Task Redundancy for Serial Robots

Various general gradient-based methods exist to solve the inverse kinematics for *serial* robots; either by augmenting the joint space [1] or by reducing the task space [2–5]. The different approaches each define a residual vector and a gradient matrix considering the properties of 3T2R tasks, e.g. by adding a virtual joint axis [1], orthogonal decomposition of the task space [2], rotation of the residual into a task frame and removing the corresponding component [4], defining the tool axis by two points for constructing a nullspace [3] or by defining the absolute orientation and the orientation residual with two reciprocal sets of Euler angles [5]. The gradient matrices corresponding to the different residuals are used for an iterative Newton-Raphson algorithm [6,7] by exploiting the functional redundancy with a null space projection of additional performance criteria [6]. Without the definition of a proper gradient, a global optimization has to be performed outside of the inverse kinematics algorithm [8,9].

1.2. Overview of Parallel Robots Structures for 3T2R tasks

Parallel robots in 3T2R tasks can be ordered in classes according to their kinematic structure into

- I mechanisms with full platform mobility (3T3R) that are redundantly controlled to five DoF,
 II mechanisms with 3T2R platform mobility enforced with a passive five-DoF constraining leg and five other legs with six DoF each,
 III mechanisms with 3T2R platform mobility resulting from the mobility of five actuated legs with five or six DoF each,
 IV mechanisms with 3T2R platform mobility and five legs with only five DoF each.

The classes I and II were introduced in [10], where class IV is analyzed regarding leg symmetry and singularities. Class III is mainly influenced by the systematic synthesis of [11] and several existing prototypes and is demarcated against class II by the absence of the passive constraining leg. Class IV can be seen as a subclass of III, but is differentiated in this paper due to its characteristics. Other classifications are provided e. g. by [12], where IV and II are termed “families”.

Examples for the first class are hexapods¹ (6UPS) [13] or the Eclipse [14] machine tool (2PPRS-PPRS). Any other parallel robot with full mobility (see e. g. [11,15,16]) may be used as well.

The second class allows for more variety, since the six-DoF mechanism and the five-DoF constraining leg can manifest in different kinematic structures: The UPS structure is used for the six-DoF part of the mechanism by [17] with a focus on kinematic analysis of 5UPS/US, by [18] with a focus on kinetostatic modeling at the example of 5UPS/RUU (see Fig. 1 a), by [19] with focus on trajectory control of 5UPS/PRPU and by [20] for pose measurement with the passive leg of 5UPS/PRPU. Other possible general base structures are RUS at the 5RUS/US example in [17], PUS, which has been investigated for the control of a redundantly actuated 6PUS/UPU regarding the control of the redundant leg with inverse-dynamics control [21] or force control [22].

The most-straightforward member of the third class is the 4UPS-UPU of Fig. 1 b, which is investigated in [23] for a simulation and feasibility study together with a survey on possible architectures for a technical realization of this class. Other possible structures are the 4URS-URU, which is analyzed kinematically in [24] and the 4PSU-PU*U, which has a special parallelogram structure in one leg (termed “U*”) and is presented in [25]. A sub-class of III consists of mechanisms [26–28], where the last joint axis of the legs is coaxial with the tool axis and is constructed as rotating ring. It contains the Metrom machine tool (4SPRR-SPR), depicted in Fig. 1 c, which is analyzed regarding inverse and forward kinematics in [26] or its variants, the redundant 4SPRR-PPSR from [28] or the hybrid 4URHU-URHR with an additional linear actuator at the platform [27]. A structural synthesis based on linear transformations and evolutionary morphology [11] led e. g. to the Isoglide5 mechanisms (3PRRRR-2PRRRR), which are analyzed and optimized regarding the isotropy of the Jacobian in [29].

The simplest member of class IV, the 5UPU is shown in [30] with the help of screw theory to only have local mobility and no global mobility, since the twist systems of the leg chains have no intersection and the resulting twist system of the platform is empty. Members of class IV have been found by systematic structural synthesis with screw theory, which has been performed in [31] for symmetric 3T2R mechanisms. The resulting 5RPUR of Fig. 1 d and 5PRUR are analyzed in [10,32].

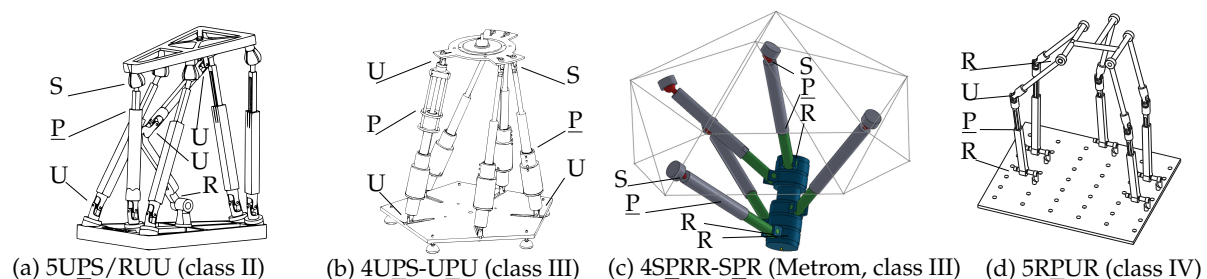


Figure 1. Typical mechanisms of the different classes. Taken from [18] (a), [23] (b), [28] (c), [10] (d).

¹ The joint structure is denoted by the number of the legs and the order of universal (“U”), prismatic (“P”), spherical (“S”), helical (“H”) and revolute (“R”) joints in the leg chains. Different actuated legs are connected by dashes (“-”), passive constraint legs are connected by a slash (“/”). Actuated joints are underlined.

In a practical application with competing requirements on workspace, stiffness, costs and precision, each of the existing systems has its legitimization. Nevertheless, each of the classes has inherent disadvantages: In tasks like milling with high process forces and requirements on stiffness and precision, robots from class II with one constraining leg have the drawback, that the passive leg takes the complete reaction wrench in the blocked rotational degree of freedom, which strongly affects the mechanisms stiffness in this direction [18]. The same is argued by [27] at the example of the Metrom machine tool, but can be extended to all the members of class III, where most leg chains have six DoF and usually only one leg chain has five DoF. This leg chain also has to take the reaction moments in the blocked DoF which affects the overall stiffness. Therefore members of the classes I and IV can be expected to reach a higher stiffness. Mechanisms of the class IV may further suffer from an increased sensitivity of manufacturing tolerances, which may cause a high pretension of the bearings or even reduce the DoF, since the five DoF of all leg chains have to coincide exactly to allow the platform to also have five DoF. Additionally, only members of class I provide redundancy which allows to use the additional DoF for performance optimizations e.g. to avoid singularities and to compensate the smaller workspace caused by the sixth leg.

Therefore, the remainder of the paper focuses on mechanisms of the first class to allow an optimization of their performance criteria using the degree of task redundancy.

1.3. Inverse Kinematics of Parallel Robots for 3T2R Tasks

The parallel robots with five DoF presented previously have a kinematic structure, that allows for an analytic model of the inverse kinematics. All references define the end-effector orientation with two consecutive elementary rotations, i.e. define two Euler angles to represent the tool axis orientation in minimal coordinates [10,19–22,26,28,32,33], which is called “partial pose” in [13]. The inverse kinematics problem (IKP) is first solved for the first chain, which is called “leading chain” in this paper. Due to the geometry of the leading chain, this solution can be found algebraically. Then the IKP is solved for the other “following” chains with the given orientation from the leading chain and standard methods. For robots of class II, the constraining leg is selected as the leading leg chain and for class III the 3T2R leg is selected.

To the best knowledge of the authors, only one reference [13] for the IKP of functionally redundant parallel robots of the class I is known. The reason presumably is that a solution of the 3T3R IKP for these robots is possible with standard methods, as used in [14] for the 3T3R Eclipse. It is always possible to transfer the 3T2R IKP into 3T3R by adding an arbitrary value for the desired rotation around the tool axis. An optimization of additional performance criteria is possible by varying the redundant rotation angle [8,9]. This approach was chosen in [13] by first defining the IKP with the redundant rotation as a parameter and then performing an optimization of this parameter using analytical computation of the dexterity and interval analysis to ensure a minimum determinant of the inverse Jacobian. The drawback of this method is the need for a cascaded optimization which is more complex than a gradient-based approach presented in this paper.

1.4. Motivation and Summary of the State of the Art

The overview over the literature shows, that no general, machine-independent methods for the resolution of functional redundancy for 3T3R PKM in 3T2R tasks exists. The works either focus on a general structural synthesis of machines e.g. via screw theory [31] or linear transformations [29] or the description and improvement of specific, manually selected, machines. To choose the best machine for given requirements, a structural synthesis is only the first step. Additionally, a dimensional synthesis should be performed for all possible structures to select the most suitable mechanism. This combined structural and dimensional synthesis [34] is sketched in Fig. 2. To be able to perform the dimensional synthesis for all structures, the inverse kinematics has to be implemented in a general form, to calculate the performance criteria over a given trajectory for further optimization of the structures and their comparison. For the generation of task redundant parallel robots, the inverse kinematics has to

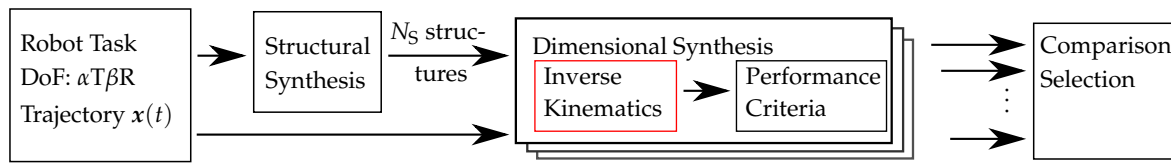


Figure 2. Overview of the procedure for combined structural and dimensional synthesis.

include an optimization of the performance criteria and the restrictions such as joint limits, to ensure a comparability of the results. To address this, the contributions of this paper are

- a general kinematics model for parallel robots using the concept of reciprocal Euler angles [5],
- a complete elimination of the redundant operational space coordinate in this formulation for 3T2R tasks allowing a nullspace optimization in the gradient-based inverse kinematics,
- proofs, examples and simulations to show the performance for single serial kinematic leg chains and complete parallel robots.

The remainder of the paper is structured as follows: The description of the inverse kinematics problem and prior definitions are given in Sec. 2 and the concept of reciprocal Euler angles from [5] is adapted in Sec. 3 for parallel robots. This leads to the full kinematic constraints of parallel robots in 3T2R tasks, introduced in Sec. 4 and applied to the differential kinematics in Sec. 5. The theoretical analysis is followed by examples and simulations in Sec. 6. The appendix contains proofs and additional details on the mathematical formulation.

2. Inverse Kinematics Problem for Parallel Robots

Before addressing the specific model for parallel robots in 3T2R tasks in the next section, the standard kinematics model of kinematics of parallel kinematic machines (“PKM”) is repeated in the following, corresponding to the state of the art [11,15,35] and serving as a reference to highlight its shortcomings for 3T2R tasks. The regarded parallel robot consists of m legs, which each have the joint coordinates q_i . All joints are considered as single-DoF and additionally to the active joints $q_{i,a}$ explicitly all passive joints at the base and at the platform $q_{i,p}$ are included in the coordinates q_i of leg i . The coordinates

$$x = \begin{bmatrix} x_t^T & x_r^T \end{bmatrix}^T \in \mathbb{R}^6 \quad (1)$$

of the end-effector platform describe the position and orientation of the end-effector frame \mathcal{F}_D with respect to the base frame \mathcal{F}_0 . In the equations, this is marked with left subscript “(0)” for vectors and left superscript “0” for rotation matrices. The platform-related end-effector frame is the desired frame in the inverse kinematics problem and is therefore abbreviated with “D”. The position

$$x_t = {}_{(0)}r_D \in \mathbb{R}^3 \quad (2)$$

is defined as the origin of the platform frame and the rotation matrix

$${}^0R_D(x_r) = \begin{bmatrix} n_D & o_D & a_D \end{bmatrix} \in \text{SO}(3) \quad (3)$$

of the platform frame is expressed with Euler angles

$$x_r = \begin{bmatrix} \beta_1 & \beta_2 & \beta_3 \end{bmatrix}^T =: \beta \in \mathbb{R}^3 \quad (4)$$

as a minimal representation of the orientation coordinates. The symbol “ β ” will be used to denote orientations relative to the base frame throughout this paper. The X-Y-Z-notation

$$R(\beta) = R_x(\beta_1)R_y(\beta_2)R_z(\beta_3) \in \text{SO}(3) \quad (5)$$

is used for the Euler angles without loss of generality. The relation between joint coordinates q and platform coordinates x is established with the kinematic constraint equations, for which most commonly the vector loop

$$\Phi_{t,i}(q_i, x) = -({}_0)r_{A_i B_i}(x) + ({}_0)r_{A_i B_i}(q_i) \quad (6)$$

between the position of the platform coupling point B_i relative to the base coupling point A_i is used for each leg chain i [15]. The second term $({}_0)r_{A_i B_i}(q_i)$ corresponds to the forward kinematics of the serial leg chain. The vector

$$({}_0)r_{A_i B_i}(x) = -({}_0)r_{A_i} + x_t + {}^0R_D(x_r)({}_D)r_{B_i} \quad (7)$$

includes the term ${}^0R_D(x_r)$ that depends on the full orientation x_r of the end-effector. For the bigger part of existing parallel robots, the passive joint coordinates can be eliminated analytically from the equations (6), e. g. by using the Euclidian distance for UPS or RPR leg chains or via trigonometry for RRR-chains. This is termed “minimal kinematics set” in [15] and leads to the scalar constraint equation

$$\Phi_i = \Phi_i(q_{i,a}, x) \quad (8)$$

for each leg i , which can be assembled to the vector of constraint equations

$$\Phi(q_a, x) = [\Phi_1 \quad \Phi_2 \quad \dots \quad \Phi_m]^T \quad (9)$$

for all m legs of the PKM. The differential kinematics of the PKM is calculated with the time derivative

$$\frac{d}{dt}\Phi(q_a, x) = \Phi_{\partial q_a} \dot{q}_a + \Phi_{\partial x} \dot{x} = 0 \quad (10)$$

where the passive joint coordinates q_p do not occur, since they have been eliminated in a previous step. The inverse-kinematics matrix²

$$\Phi_{\partial q_a} = \frac{\partial \Phi}{\partial q_a} = \begin{bmatrix} \Phi_{1,\partial q_{1,a}} & 0 & 0 & 0 \\ 0 & \Phi_{2,\partial q_{2,a}} & \ddots & 0 \\ 0 & \ddots & \ddots & 0 \\ 0 & 0 & 0 & \Phi_{m,\partial q_{m,a}} \end{bmatrix} \quad (11)$$

of this model has diagonal form and the direct-kinematics matrix

$$\Phi_{\partial x} = \frac{\partial \Phi}{\partial x} = \begin{bmatrix} \partial \Phi_1 / \partial x \\ \partial \Phi_2 / \partial x \\ \vdots \\ \partial \Phi_m / \partial x \end{bmatrix} \quad (12)$$

is fully populated. This definition of the constraints has the following drawbacks:

1. For parallel robots with arbitrary leg chains like those generated by a structural synthesis [11,31,34], it is generally not possible to analytically eliminate the passive joint coordinates.
2. If more than three joint coordinates per leg influence the coupling point position B_i , the three kinematic constraints per joint in (6) are not sufficient to generate enough equations for the matrix of (11) to become invertible. The velocity-based theory of linear transformations used by

² We follow the argumentation from [11] to avoid the term “Jacobian”, since the matrix is not a Jacobian in the mathematical sense to project between two spaces. The name results from the inversion of this matrix in the inverse kinematics problem.

[11] allows to determine the mobility of arbitrary parallel robots. The linear transformation is generalized in [12] to accuracy and stiffness modeling by means of screw theory resulting in the “generalized Jacobian”. Both concepts do not provide a direct appliance to solve the IKP, since this requires a formulation of the orientation at position level, not velocity level.

3. Exploiting the reduction of end-effector coordinates for 3T2R tasks is not possible, since all end-effector coordinates are included in (7).

An alternative kinematic model to encounter the combination of these points is presented in the next section, where the concept of reciprocal sets of Euler angles for the inverse kinematics problem for serial link robots [5] is transferred to the leading leg of parallel robots.

3. Reciprocal Sets of Euler Angles for the Kinematics of a Serial Leg Chain

To take the rotational symmetry around the tool axis in 3T2R tasks into account, a new set of task space coordinates

$$\eta = \begin{bmatrix} \eta_t^T & \eta_r^T \end{bmatrix}^T \in \mathbb{R}^5 \quad (13)$$

has to be defined. The translational part

$$\eta_t = x_t = {}_{(0)}r_D \in \mathbb{R}^3 \quad (14)$$

remains unchanged relative to the operational space coordinates x . The rotational part

$$\eta_r = \begin{bmatrix} \beta_1 & \beta_2 \end{bmatrix}^T = \underbrace{\begin{bmatrix} 1 & 0 & 0 \\ 0 & 1 & 0 \end{bmatrix}}_{=P_{\eta_r}} x_r \in \mathbb{R}^2 \quad (15)$$

only contains the first two rotational coordinates of x . The last operational space coordinate β_3 , the rotation around the z -axis a_D of \mathcal{F}_D , is excluded from the task space by the selection matrix P_{η_r} . To be able to set the rotational DoF around the tool axis in 3T2R tasks arbitrarily and use gradient-based inverse kinematics, β_3 has to be eliminated completely from the kinematics equations (6). To simplify the following elaborations, the platform frame \mathcal{F}_D is still identified as the desired frame of the inverse kinematics problem and the end-effector frame that results from the joint angles of leg i is now termed \mathcal{F}_E , which corresponds to the forward kinematics of the leg chain. For a formulation without the tool axis rotation, a different constraint definition

$$\Phi_{t,i}(q_i, x) = -{}_{(0)}r_D + {}_{(0)}r_E(q_i) = -x_t + {}_{(0)}r_E(q_i) \in \mathbb{R}^3 \quad (16)$$

containing the vector loop from the robot base frame \mathcal{F}_0 to the platform \mathcal{F}_D and the leg chain end-effector \mathcal{F}_E can be used, where in contrast to (6) only the translational part x_t of the end-effector coordinates appears and not the rotational part x_r . The vector loop is depicted in Fig. 3 for a planar robot with opened (Fig. 3 a, b) and closed loops (Fig. 3 c). The triangle represents the end-effector platform and only one leg chain is drawn in the figure.

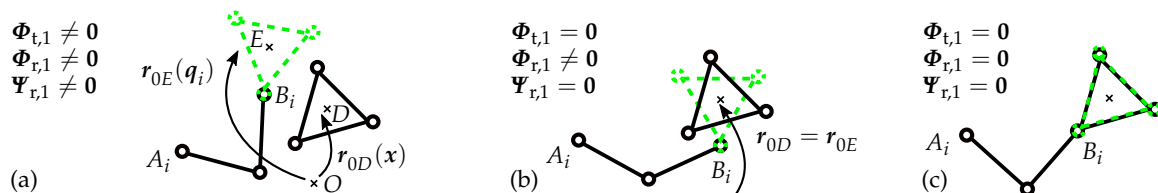


Figure 3. Different cases for the kinematic constraints of the leading chain for the 3RRR example: (a) no constraints complied; (b) position and tool axis rotation complied; (c) all constraints complied.

As a drawback of (16), all joint angles q_i of the leg i and not only the coordinates of the first joints counted from the base are now included in the vector

$${}^{(0)}\mathbf{r}_E(q_i) = {}^{(0)}\mathbf{r}_{A_i} + {}^{(0)}\mathbf{r}_{A_i B_i}(q_i) + {}^0\mathbf{R}_{B_i}(q_i)_{(B_i)}\mathbf{r}_E. \quad (17)$$

This implies, that the platform is now part of the last link of the considered leg chain, as sketched in Fig. 3 by the dashed triangle. To account for the increased number of included joints in (17), the full kinematic constraints

$$\Phi_i = \begin{bmatrix} \Phi_{t,i}^T & \Phi_{r,i}^T \end{bmatrix}^T \in \mathbb{R}^6, \quad (18)$$

have to be considered, including the rotational part

$$\Phi_{r,i}(q_i, \mathbf{x}) = \begin{bmatrix} \alpha_1 & \alpha_2 & \alpha_3 \end{bmatrix}^T = \alpha \left({}^D\mathbf{R}_E(\mathbf{x}_r, q_i) \right) = \alpha \left({}^0\mathbf{R}_D^T(\mathbf{x}_r) {}^0\mathbf{R}_E(q_i) \right), \quad (19)$$

which is needed to generate enough equations for an invertible matrix in the differential equations. The constraints again contain the deviation between the desired end-effector frame \mathcal{F}_D expressed with \mathbf{x} and the actual robots end-effector frame \mathcal{F}_E expressed with q . Fig. 3 (b) and (c) show cases, where the translational constraints are met, but the rotational constraints have different values. For 3T3R tasks, only Fig. 3 (c) represents a valid solution of the inverse kinematics. For 3T2R tasks, Fig. 3 (b) and (c) represent valid solutions.

The goal of eliminating the tool rotation β_3 from the equations is not achieved yet, since all three components of the platform orientation \mathbf{x}_r affect the rotation matrix ${}^0\mathbf{R}_D$. This can be addressed by the selection of the Euler angles: Similar to the definition of the rotational operational space coordinates \mathbf{x}_r in (4), the constraints $\Phi_{r,i}$ are also expressed with a set of Euler angles α . In the following, “ α ” will always refer to the rotation error/residual and “ β ” to an orientation relative to the base frame. The Euler angle convention of α can be chosen independently of the choice for the orientation representation in β . The intuitive approach of choosing

$$\mathbf{R}(\alpha^*) := \mathbf{R}_x(\alpha_1^*)\mathbf{R}_y(\alpha_2^*)\mathbf{R}_z(\alpha_3^*) \in \text{SO}(3) \quad (20)$$

the same way as β leads to a set of transformations depicted in Fig. 4 (a) where the intermediate steps of the single elementary rotations are omitted since they have no technical meaning. The upperscript asterisk in (20) demarcates this specific example and the following elaborations on the calculation of α .

To be able to remove the redundant coordinate β_3 from the rotational constraints of (19), it is necessary to change the expression of the orientation error α to be reciprocal to the expression of the absolute orientation β . By using the Z-Y-X-Euler angles with

$$\mathbf{R}(\alpha) := \mathbf{R}_z(\alpha_1)\mathbf{R}_y(\alpha_2)\mathbf{R}_x(\alpha_3) \in \text{SO}(3) \quad (21)$$

only the error component α_1 is affected by rotations around the tool axis, which is the z-axis of the intermediate frames \mathcal{F}_{A1} , \mathcal{F}_{A2} and the platform frame \mathcal{F}_D in Fig. 4 (b), where the frame rotations with

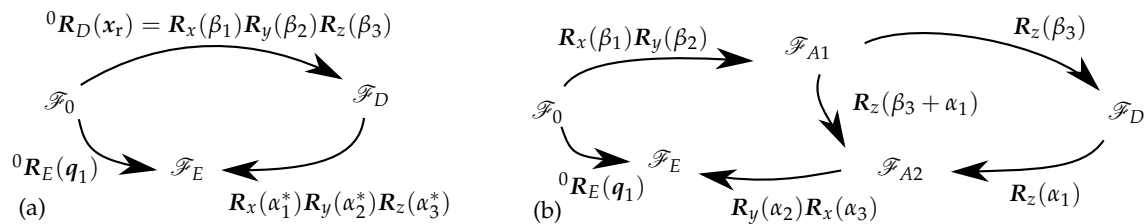


Figure 4. Overview of the different frames (a) for six-DoF tasks with standard Euler angle notation and (b) for five-DoF tasks with reciprocal Euler angle notation; taken from [5].

the reciprocal set of Euler angles are sketched. The mathematical proof is given in appendix A.1 and in [5]. The new, reduced rotational part of the kinematic constraints

$$\Psi_{r,i}(q_i, \eta) = \begin{bmatrix} \alpha_2 & \alpha_3 \end{bmatrix}^T = \overbrace{\begin{bmatrix} 0 & 1 & 0 \\ 0 & 0 & 1 \end{bmatrix}}^{=P_{\Psi_r}} \Phi_{r,i}(q_i, x) \in \mathbb{R}^2 \quad (22)$$

does not contain the tool rotation any more. The full kinematic constraints for the reduced coordinates

$$\Psi_i = \begin{bmatrix} \Phi_{t,i}^T & \Psi_{r,i}^T \end{bmatrix}^T \in \mathbb{R}^5 \quad (23)$$

can be used for the inverse kinematics of the leg chain i in 3T2R tasks, where $\Psi_i = \mathbf{0}$ leads to a valid position and orientation of the tool axis. The condition $\Phi_i = \mathbf{0}$ leads to a valid configuration of leg i of the parallel robot in 3T3R tasks. In the following, “ Φ ” is always used for 3T3R³ kinematic descriptions and “ Ψ ” for 3T2R.

4. Full Kinematic Constraints for Parallel Robots using Reciprocal Sets of Euler Angles

The definition of the full kinematic constraints (16,19,18) of a single leg chain of the parallel robot from the previous chapter can be used to write the kinematic constraints in a general form. The full kinematic constraint equations can only be defined for 3T3R tasks without further adaptations as

$$\Phi = \begin{bmatrix} \Phi_1^T & \Phi_2^T & \dots & \Phi_m^T \end{bmatrix}^T. \quad (24)$$

The constraints Ψ_i from (23) for the reduced coordinates η can only be defined for one leg chain: Fig. 5 (a) show an open-loop second leg chain for a given first leg chain from Fig. 3. By also closing the 3T2R kinematic constraints Ψ_2 for the second loop, as depicted in Fig. 5 (b), the tool axis stays arbitrary and the platform pose demanded from the two legs would be different and therefore would not be a valid solution for the complete mechanism, i.e. $\Phi_2 \neq \mathbf{0}$. Only if the second leg fulfills the 3T3R kinematic constraints for all platform coordinates, as shown in Fig. 5 (c), a valid configuration of the mechanism emerges. This approach has already been used for many specific robots systems, as introduced in Sec. 1. As a generalization, the first leg of the parallel robot is now termed the “leading leg chain” (Index “1”) and the other legs are termed as “following leg chains” (Index “ j ”).

The translational part of the constraints is not coupled by the platform orientation and therefore left unchanged relative to (16) with

$$\Phi_{t,j}(q_j, x) = -{}_{(0)}r_D + {}_{(0)}r_E(q_j) = -x_t + {}_{(0)}r_E(q_j) \in \mathbb{R}^3 \quad (25)$$

³ By omitting the corresponding lines in the operational space coordinates x and the constraint equations Φ , it is also possible to use the 3T3R approach for systems with reduced mobility of 2T1R, 3T0R and 3T1R platform DoF.

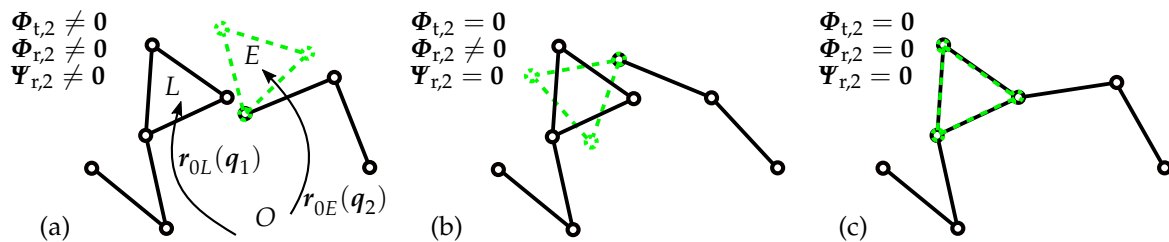


Figure 5. Different cases for the kinematic constraints of the following chain: (a) wrong position and orientation; (b) correct position and wrong orientation; (c) all kinematic constraints are complied.

for the following legs j . The orientation for the platform is given with the rotation matrix

$${}^0R_L(q_1) := {}^0R_E(q_1) \quad (26)$$

which gives the reference end-effector frame \mathcal{F}_L resulting from the leading leg 1. The rotational part of the kinematic constraints

$$\Phi_{r,j}(q_j, q_1) = \alpha ({}^0R_L^T(q_1) {}^0R_E(q_j)) \quad (27)$$

for the following leg is given by the Euler angle representation of the deviation between the orientation of the platform frame \mathcal{F}_L given by the leading (“L”) leg and the frame \mathcal{F}_E given by the respective following leg j . The choice of the Euler angle notation is arbitrary. The full kinematic constraints for the complete parallel robot with m legs for 3T2R tasks

$$\Psi = \begin{bmatrix} \Psi_1^T & \Phi_2^T & \dots & \Phi_m^T \end{bmatrix}^T \quad (28)$$

are assembled from the 3T2R constraints Ψ_1 from (23) for the leading leg and the 3T3R constraints Φ_j , $2 \leq j \leq m$ from (25,27) for the following legs. The index “ j ” is used to distinguish the following legs of the 3T2R case and all legs “ i ” of the general case in Sec. 3. The full constraints of (28) lead to a 35-dimensional vector for the kinematic constraints for parallel robots with six legs in 3T2R tasks, which are aggregated as class I in Sec. 1.2. This formulation can be reduced by combining the mechanism-specific approach for the constraints from (6) with the principle of leading and following legs of this section. For the 6UPS structure this would result in a 10-dimensional constraint vector with five entries for the leading leg and only one entry for each following leg.

5. Differential Kinematics for Parallel Robots

To be able to compute the differential kinematics of the constraints Φ (24) and Ψ (28) to

$$\frac{d}{dt} \Phi(q, x) = \Phi_{\partial q} \dot{q} + \Phi_{\partial x} \dot{x} = 0 \quad \text{and} \quad \frac{d}{dt} \Psi(q, \eta) = \Psi_{\partial q} \dot{q} + \Psi_{\partial \eta} \dot{\eta} = 0, \quad (29)$$

the full geometric matrices of inverse kinematics

$$\Phi_{\partial q}(q, x) = \begin{bmatrix} \Phi_{1,\partial q_1} & 0 & 0 & 0 \\ 0 & \Phi_{2,\partial q_2} & \ddots & 0 \\ \vdots & \ddots & \ddots & 0 \\ 0 & 0 & 0 & \Phi_{m,\partial q_m} \end{bmatrix} \quad \text{and} \quad \Psi_{\partial q}(q, \eta) = \begin{bmatrix} \Psi_{1,\partial q_1} & 0 & 0 & 0 \\ \Phi_{2,\partial q_1} & \Phi_{2,\partial q_2} & \ddots & 0 \\ \vdots & \ddots & \ddots & 0 \\ \Phi_{m,\partial q_1} & 0 & 0 & \Phi_{m,\partial q_m} \end{bmatrix} \quad (30)$$

and the full geometric matrices of direct kinematics

$$\Phi_{\partial x}(q, x) = \frac{\partial \Phi}{\partial x} = \begin{bmatrix} \Phi_{1,\partial x} \\ \Phi_{2,\partial x} \\ \vdots \\ \Phi_{m,\partial x} \end{bmatrix} \quad \text{and} \quad \Psi_{\partial \eta}(q, \eta) = \frac{\partial \Psi}{\partial \eta} = \begin{bmatrix} \Psi_{1,\partial \eta} \\ \Phi_{2,\partial \eta} \\ \vdots \\ \Phi_{m,\partial \eta} \end{bmatrix} \quad (31)$$

have to be calculated for the 3T3R and the 3T2R case respectively. The gradient $\Phi_{\partial q}$ has block diagonal form, indicating that the inverse kinematics problem can be solved for each leg independently. The structures of the gradient $\Psi_{\partial q}$ results from the coupling of the leading and following joints in the rotational constraints equation.

The gradient matrices $\Phi_{\partial q}$ and $\Phi_{\partial x}$ contain nested nonlinear functions related to the orientation error, therefore the geometric Jacobian of the leg chains can not be exploited for the rotational part, as derived in appendix A.2. The gradients are calculated with the chain rule and a syntax for stacking

matrix columns to avoid differentiating matrices or with respect to matrices, which was introduced in [5]. The product operator $\overline{\Pi}$, the stacking operator \overline{R} and the transpose operator P_T used for the implementation in the next section are explained in appendix A.3.

5.1. Constraint Gradients for the Leading Leg of the 3T2R and all Legs of the 3T3R case

The constraint definition Ψ_1 for the leading leg of the 3T2R case (28) and Φ_i with $i = 1, \dots, m$ for all legs of the 3T3R case (24) are subject to the same model of (16,19,18). In the following, the 3T3R constraints are displayed. The form Ψ_1 for the 3T2R case is obtained by removing the corresponding line of the rotational component according to (22) and replacing “ Φ ” by “ Ψ ” in the following equations. For the analysis, the constraint gradient matrix w. r. t. the joint coordinates has to be divided out to

$$\Phi_{1,\partial q_1} = \begin{bmatrix} \Phi_{t,1,\partial q_1}^T & \Phi_{r,1,\partial q_1}^T \end{bmatrix}^T, \quad (32)$$

where the translational component can be calculated with the geometric Jacobian of the leg chain, as derived in appendix A.2. The rotational part is written down as a function composition of the three functions α (Euler angles), $\overline{\Pi}$ (matrix product) and 0R_E (rotation matrix) as

$$\Phi_{r,1,\partial q_1} = \frac{\partial}{\partial q_1} \alpha \left({}^0R_D^T(x) {}^0R_E(q_1) \right) = \frac{\partial}{\partial q_1} \alpha \left(\overline{\Pi} \left({}^0\overline{R}_D^T(x), {}^0\overline{R}_E(q_1) \right) \right), \quad (33)$$

which is then expanded with the chain rule for differentiation and the stack operators to

$$\Phi_{r,1,\partial q_1} = \underbrace{\frac{\partial \alpha}{\partial \overline{R}}}_{I \in \mathbb{R}^{3 \times 9}} \underbrace{\frac{\partial \overline{\Pi} \left({}^0\overline{R}_D^T, {}^0\overline{R}_E \right)}{\partial {}^0\overline{R}_E}}_{II \in \mathbb{R}^{9 \times 9}} \underbrace{\frac{\partial {}^0\overline{R}_E(q_1)}{\partial q_1}}_{III \in \mathbb{R}^{9 \times \dim(q_1)}} \in \mathbb{R}^{3 \times \dim(q_1)}. \quad (34)$$

The two first partial derivatives from (34) are sparse matrices and can be calculated efficiently as shown in appendix A.3. The factor “I” contains (A20) with $\overline{R} = {}^D\overline{R}_E(x_r, q_1)$ and the factor “II” is (A23) with the contents of ${}^0\overline{R}_D^T(x_r)$. The last partial derivative “III” can be derived with computer algebra systems from the analytic expression of the rotation matrix ${}^0R_E(q_1)$. The leading legs constraint gradient matrix w. r. t. the platform coordinates can be expanded in the same manner into

$$\Phi_{1,\partial x} = \begin{bmatrix} \Phi_{t,1,\partial x_t} & \Phi_{t,1,\partial x_r} \\ \Phi_{r,1,\partial x_t} & \Phi_{r,1,\partial x_r} \end{bmatrix} = \begin{bmatrix} -1 & 0 \\ 0 & \Phi_{r,1,\partial x_r} \end{bmatrix}, \quad (35)$$

where the definitions from (16) and (19) only leave the rotational part

$$\begin{aligned} \Phi_{r,1,\partial x_r} &= \frac{\partial}{\partial x_r} \alpha \left(\left({}^0R_E^T(q_1) {}^0R_D(x_r) \right)^T \right) = \frac{\partial}{\partial x_r} \bar{\alpha} \left(P_T \overline{\Pi} \left({}^0\overline{R}_E^T(q_1), {}^0\overline{R}_D(x_r) \right) \right) \\ &= \underbrace{\frac{\partial \bar{\alpha}}{\partial \overline{R}}}_{I \in \mathbb{R}^{3 \times 9}} \underbrace{P_T}_{II \in \mathbb{R}^{9 \times 9}} \underbrace{\frac{\partial \overline{\Pi} \left({}^0\overline{R}_E^T, {}^0\overline{R}_D \right)}{\partial {}^0\overline{R}_D}}_{III \in \mathbb{R}^{9 \times 9}} \underbrace{\frac{\partial {}^0\overline{R}_D(x_r)}{\partial x_r}}_{IV \in \mathbb{R}^{9 \times 3}} \in \mathbb{R}^{3 \times 3}, \end{aligned} \quad (36)$$

where the simplicity of the single expression “I”-“IV” is demonstrated in appendix A.3. The factors are (A20) with $\overline{R} = {}^D\overline{R}_E(x_r, q_1)$ in “I”, the permutation matrix for transposition from (A19) in “II”, (A23), where the contents of ${}^0\overline{R}_E^T$ are inserted in “III” and (A21) with the elements of x_r for β in “IV”.

5.2. Constraint Gradients for the Following Leg in the 3T2R Case

As explained regarding (24), the constraints (16) and (19) and their gradients (34) and (36) are used for all legs in the 3T3R case and the leading leg in the 3T2R case. For the following legs in the

3T2R case, the gradients $\Phi_{j,\partial q_1}$, $\Phi_{j,\partial q_j}$ and $\Phi_{j,\partial x}$ with $j = 2, \dots, m$ from the right part of (30) and (31) have to be calculated in a similar way. Due to the absence of the platform orientation in (27), (35) simplifies for the following leg to

$$\Phi_{j,\partial x} = \begin{bmatrix} -1 & 0 \\ 0 & 0 \end{bmatrix}. \quad (37)$$

The gradient w. r. t. the joint coordinates of the following leg contains again the translational part of the legs Jacobian regarding the end-effector platform position in $\Phi_{t,j,\partial q_j}$ and has the rotational part

$$\begin{aligned} \Phi_{r,j,\partial q_j} &= \frac{\partial}{\partial q_j} \alpha \left({}^0 R_L^T(q_1) {}^0 R_E(q_j) \right) = \frac{\partial}{\partial q_j} \alpha \left(\overline{\Pi} \left({}^0 \overline{R}_L^T(q_1), {}^0 \overline{R}_E(q_j) \right) \right) \\ &= \underbrace{\frac{\partial \alpha}{\partial \overline{R}}}_{I \in \mathbb{R}^{3 \times 9}} \underbrace{\frac{\partial \overline{\Pi} \left({}^0 \overline{R}_D^T, {}^0 \overline{R}_E \right)}{\partial {}^0 \overline{R}_E}}_{II \in \mathbb{R}^{9 \times 9}} \underbrace{\frac{\partial {}^0 \overline{R}_E(q_j)}{\partial q_j}}_{III \in \mathbb{R}^{9 \times \dim(q_j)}} \in \mathbb{R}^{3 \times \dim(q_j)}, \end{aligned} \quad (38)$$

which is similar to the expression in (34). The factors of the equation (38) are (A20) with $\overline{R} = {}^L \overline{R}_E(q_1, q_j)$ in “I”, (A23), where the elements of ${}^0 R_L^T(q_1)$ have to be inserted in “II” and the partial derivative of the platform orientation calculated from leg j w. r. t. the legs joint coordinates in “III”, similar to term “III” from (34). The gradient w. r. t. the joint coordinates of the leading leg

$$\begin{aligned} \Phi_{r,j,\partial q_1} &= \frac{\partial}{\partial q_1} \alpha \left(\left({}^0 R_E^T(q_j) {}^0 R_L(q_1) \right)^T \right) = \frac{\partial}{\partial q_1} \alpha \left(P_T \overline{\Pi} \left({}^0 \overline{R}_E^T(q_j) {}^0 \overline{R}_L(q_1) \right) \right) \\ &= \underbrace{\frac{\partial \alpha}{\partial \overline{R}}}_{I \in \mathbb{R}^{3 \times 9}} \underbrace{P_T}_{II \in \mathbb{R}^{9 \times 9}} \underbrace{\frac{\partial \overline{\Pi} \left({}^0 \overline{R}_E^T, {}^0 \overline{R}_L \right)}{\partial {}^0 \overline{R}_L}}_{III \in \mathbb{R}^{9 \times 9}} \underbrace{\frac{\partial {}^0 \overline{R}_L(q_1)}{\partial q_1}}_{IV \in \mathbb{R}^{9 \times \dim(q_1)}} \in \mathbb{R}^{3 \times \dim(q_1)}. \end{aligned} \quad (39)$$

is similar to the expression in (36). The order of the residual expression (27) has to be switched by exploiting the associative property of matrix transposition to avoid differentiating a transposed matrix. The factors of equation (39) are (A20) with $\overline{R} = {}^L \overline{R}_E(q_1, q_j)$ in “I”, the permutation matrix for transposition from (A19) in “II”, (A23) with ${}^0 \overline{R}_E^T(q_j)$ in “III” and the term “III” from (34) in “IV”.

5.3. Gradient-Based Solution of the Inverse Kinematics Problem with Redundancy Resolution

The presented kinematic constraints and their gradient matrices can be used to solve the inverse kinematics problem (IKP) of single leg chains and complete parallel robots. Since all active and passive joint angles are involved for the case of parallel robots, solving their IKP results in solving the IKP for all leg chains. As first introduced in [7] for Euler angle residuals in the IKP, the Taylor series expansion of $\Phi(q, x)$ leads to the definition of

$$\Phi(q^{k+1}, x) = \Phi(q^k, x) + \frac{\partial}{\partial q} \Phi(q, x) \Big|_{q^k} (q^{k+1} - q^k) \quad (40)$$

in an iterative algorithm at the step $k + 1$, which can be used to solve the IKP using a given initial value q^0 and the condition

$$\Phi(q^{k+1}, x) = 0. \quad (41)$$

Defining the solution of the IKP as the main task (“T”), the step-wise solution for the joint coordinates results to

$$\Delta q^k = \Delta q_T^k = q^{k+1} - q^k = -\Phi_{\partial q}^+(q^k, x) \Phi(q^k, x). \quad (42)$$

208 Depending on the dimension, $(\cdot)^+$ denotes the matrix inverse or the pseudo-inverse. Again, the
 209 equations (40-42) can be written with “ Ψ ” from (28) instead of “ Φ ” from (24) for the 3T2R case.

In the latter case, the corresponding gradient matrix $\Psi_{\partial q}(q, \eta)$ from (30) allows the definition of a nullspace in the case of $\dim(q_1) > \dim(\eta)$. This redundancy can be exploited by using the nullspace (“N”) projection Δq_N from [6] additionally to the solution Δq_T of the IKP in (42) with the new increment

$$\Delta q^k = q^{k+1} - q^k = \Delta q_T^k + \Delta q_N^k = -\Psi_{\partial q}^\dagger \Psi + (1 - \Psi_{\partial q}^\dagger \Psi_{\partial q}) h_{\partial q} \quad (43)$$

in the iterative algorithm. The optimization of additional performance criteria h requires their gradient $h_{\partial q}$ w. r. t the joint positions. One criterion is the summed W_1 -weighted quadratic distance

$$h_1(q) = \frac{1}{2}(q - \bar{q})^T W_1 (q - \bar{q}), \quad h_{1,\partial q} = \frac{\partial h_1}{\partial q} = W_1 (q - \bar{q}) \quad (44)$$

of the joint positions q from their respective reference position \bar{q} , e. g. used in [2,36]. Defining \bar{q} to be in the middle of the joint limits and minimizing $h_1(q)$ reduces the risk of joints reaching their technical limits, but does not guarantee it, since exceeding the limit for one joint can be compensated by improving other joints. The W_2 -weighted hyperbolic joint limit distance

$$h_2(q) = \frac{1}{n} \sum_{i=1}^n w_{2,i} \frac{(q_{i,\max} - q_{i,\min})}{8} \left(\frac{1}{(q_i - q_{i,\min})^2} + \frac{1}{(q_i - q_{i,\max})^2} \right) \quad (45)$$

from [8] (written element-wise for $n = \dim(q)$) circumvents this problem by generating infinitely high values when reaching the limits. In contrast to h_1 , the criterion h_2 is only defined for joints within their limits with $q_{i,\min} < q_i < q_{i,\max}$, which is ensured by setting $w_{2,i} = 0$ for joints exceeding their limits and $w_{2,i} = 1$ otherwise. To combine the effect of drawing joint positions to their middle with h_1 of (44) and of strongly rejecting joints directly near their limits with h_2 of (45), their weighted sum

$$h_3(q) = K_{h_1} h_1(q) + K_{h_2} h_2(q) \quad (46)$$

210 is used in the simulation studies of Sec. 6. Other criteria not related to the joint limits are for example
 211 stiffness [9] or singularity avoidance via Frobenius-norm condition number [8] or squared condition
 212 number [3]. The method can be used for serial link robots as well by removing all entries for the
 213 following legs from the formulas, as presented in [5]. The platform pose x/η corresponds to the desired
 214 pose for the serial robots end-effector and the kinematic constraints Φ/Ψ correspond to the residual of
 215 the IKP.

In the practical implementation, it has proven to be useful to extend the basic principle of (43) to

$$\Delta q^k = K_{\text{Lim}}(q^k) K_{\text{Rel}}(q^k) (K_T \Delta q_T^k + K_N \Delta q_N^k), \quad (47)$$

216 where the constant damping coefficients K_T for Δq_T^k and K_N for Δq_N^k were introduced to avoid
 217 overshooting of the solution for the prize of slower convergence. The damping term K_N has to
 218 be chosen according to the optimization criterion. Further damping was introduced for the 3T2R
 219 case with task redundancy to reduce a Δq^k that would lead to overshoot over the joint limits with
 220 $K_{\text{Lim}}(q^k)$. The value $K_{\text{Lim}} = 1$ is set if no limits would be violated by the increment Δq^k . For the 3T3R
 221 case, $K_{\text{Lim}} := 1$ is set permanently, since slowing down when approaching the limits does not change
 222 the direction of the increment and violating the limits is inevitable. The maximum step size for one
 223 iteration Δq^k was ensured with $K_{\text{Rel}}(q^k)$ to stay below 5 % of the joint limit range to prevent leaving the
 224 validity of the first-order linearization of (40). For smaller increments, $K_{\text{Rel}} = 1$ holds. The damping
 225 terms are always applied to the full vector and not to single elements and therefore only change the
 226 norm and not the direction of Δq^k .

5.4. Differential Kinematics for the Parallel Robot and its Applications

The reasonings so far only considered the inverse kinematics of the parallel robot. The kinematic definitions can also be used in the differential kinematics (29) to establish the connection between joint and platform velocity. This was already presented in general form in [15] and also corresponds to the theory of linear transformation which is the base of the works of Gogu on structural synthesis [11]. The derivation in this paper is based on the position *and* orientation, but comes to the same result as the already-existing velocity-based approach. Further, using Ψ/η as elaborated before allows for the first time to define differential kinematics specifically for 3T2R tasks in a general form. The differential equation of (29) is expanded to

$$\frac{d}{dt} \Phi(q_a, q_p, x) = \Phi_{\partial q_a} \dot{q}_a + \Phi_{\partial q_p} \dot{q}_p + \Phi_{\partial x} \dot{x} = 0 \quad (48)$$

to distinguish active (“a”) and passive (“p”) joints. The latter also contain the coordinates of the platform-connecting joints. Reordering the equation leads to the full inverse differential kinematics

$$\Phi_{\partial x} \dot{x} = - \begin{bmatrix} \Phi_{\partial q_a} & \Phi_{\partial q_p} \end{bmatrix} \begin{bmatrix} \dot{q}_a \\ \dot{q}_p \end{bmatrix} = \Phi_{\partial ap} \begin{bmatrix} \dot{q}_a \\ \dot{q}_p \end{bmatrix}, \quad \begin{bmatrix} \dot{q}_a \\ \dot{q}_p \end{bmatrix} = -\Phi_{\partial ap}^{-1} \Phi_{\partial x} \dot{x}, \quad (49)$$

which has been addressed in the previous sections, and the full direct differential kinematics

$$\Phi_{\partial q_a} \dot{q}_a = - \begin{bmatrix} \Phi_{\partial x} & \Phi_{\partial q_p} \end{bmatrix} \begin{bmatrix} \dot{x} \\ \dot{q}_p \end{bmatrix} = \Phi_{\partial xp} \begin{bmatrix} \dot{x} \\ \dot{q}_p \end{bmatrix}, \quad \begin{bmatrix} \dot{x} \\ \dot{q}_p \end{bmatrix} = -\Phi_{\partial xp}^{-1} \Phi_{\partial q_a} \dot{q}_a. \quad (50)$$

By only selecting the first rows for \dot{q}_a in (49) and for \dot{x} in (50), the well-known analytic Jacobian⁴ of the parallel robot [11,15], relating actuator velocities \dot{q}_a and platform velocities \dot{x} , can be obtained from both equations. For the case of task or kinematic redundancy, the pseudo-inverse can be used for $\Phi_{\partial ap}$ in (49) as shown in Sec. 5.3. The case of task redundancy does not affect (50), since the full platform velocity \dot{x} is obtained from given actuator velocities \dot{q}_a .

6. Results

To evaluate the inverse kinematics algorithm presented in the previous section 5.3, first the solution of the IKP is shown for the trajectory of a serial-link industrial robot in Sec. 6.1 and for the trajectory of a parallel robot in Sec. 6.2. The results are generalized by the statistical analysis of random point-to-point movements of arbitrary serial link chains in Sec. 6.3.

6.1. Resolution of Functional Redundancy of a Serial-Link Six-DoF Robot in 3T2R tasks

The first evaluation of the inverse kinematics algorithm from Sec. 5.3 is performed with simulations at the basic example of a six-DoF industrial robot with a rectangular trajectory. The manipulator Fanuc M-710 iC/50 was taken from the example of [36] with the tabulated kinematics parameters and a sketch of the trajectory in Fig. 6. Deviations in the parameters relative to [36] result from the use of the *modified* Denavit-Hartenberg⁵ notation for the joint transformation according to KHALIL and the use of only positive α_i parameters for axis alignment for consistency with the results of the structural synthesis from [34]. The trajectory is a rectangle with 500 mm \times 800 mm and a desired alignment of the z-axis pointing into the ground plane.

⁴ This matrix is related to the time derivatives \dot{x}_r of the platform Euler angles and is called “design Jacobian” in [11] and “Euler angles inverse jacobian matrix” in [15] in contrast to the Jacobian related to angular velocities of the platform.

⁵ The four DH parameters contain the minimal set of kinematic parameters for single joint transformations which correspond to distances and angle offsets between joint axes.

i	α_i R _x	d_i T _x	θ_i R _z	r_i T _z	$q_{i,\min}$	$q_{i,\max}$
1	0	0	q_1	0	-180°	180°
2	90°	150 mm	q_2	0	30°	165°
3	0	870 mm	q_3	0	-132°	230°
4	90°	170 mm	q_4	1016 mm	-360°	360°
5	90°	0	q_5	0	-125°	125°
6	90°	0	q_6	-175 mm	-360°	360°

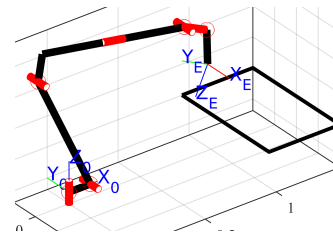


Figure 6. Left: Table with the kinematic parameters of the industrial manipulator Fanuc M-710 iC/50. Right: sketch of the robot scenario.

The IKP is solved with two settings: Setting the tool axis rotation to different constant values β_3 with the 3T3R algorithm and solving the IKP only for the desired pointing direction with the 3T2R algorithm. The algorithm from (43) was used in the extended version of (47) for both cases with different settings caused by their nature. For the 3T3R case, $K_T = 0.7$ and $K_N = 0.7$ were set. The terms K_N and K_{Lim} have no effect, since no nullspace movement is possible. For the 3T2R case, with $K_{h_1} = 0$ and $K_{h_2} = 1$ only the hyperbolic limit rejection criterion from (45) was used. The first criterion was not used, since in the trajectory example the limits are not even temporarily exceeded by principle. All IKP algorithms had the same initial value from Fig. 6.

The results of the inverse kinematics for different settings are given in Fig. 7, where the representative joint coordinates q_1 and q_5 , the redundant coordinate of the end-effector orientation β_3 , as well as the optimization criterion (45) are depicted over time for the trajectory from Fig. 6. The positions are normalized to the joint limits from -1 to 1. The first three lines in Fig. 7 represent IKP solutions with a given constant end-effector orientation β_3 of -150°, -15° and 45° and the 3T3R algorithm. The 3T2R algorithm without nullspace optimization is plotted with dotted lines for each first sample of the 3T3R cases as initial value with the same colors. Using these initial values for a 3T2R IK with optimization leads to strong nullspace movements at the beginning, quickly converging to a local minimum. Therefore the 3T2R case with optimization, plotted as the green line with triangle markers, is shown only for the initial condition from Fig. 6. It can be observed, that the optimization of the criterion leads to the best solution of the IKP. The lines for the criterion for $\beta_3 = -150^\circ$ and $\beta_3 = -15^\circ$ partly exceed the limits of the plot, indicating that the limit is violated, which can also be seen at the plot for q_5 . This exposes the need for keeping the solution always within the limits by the measures described. The 3T2R IK without optimization with dotted lines tends to lower changes in the joint positions than the 3T3R IK, since this corresponds to the solution of the matrix pseudo-inverse in (43).

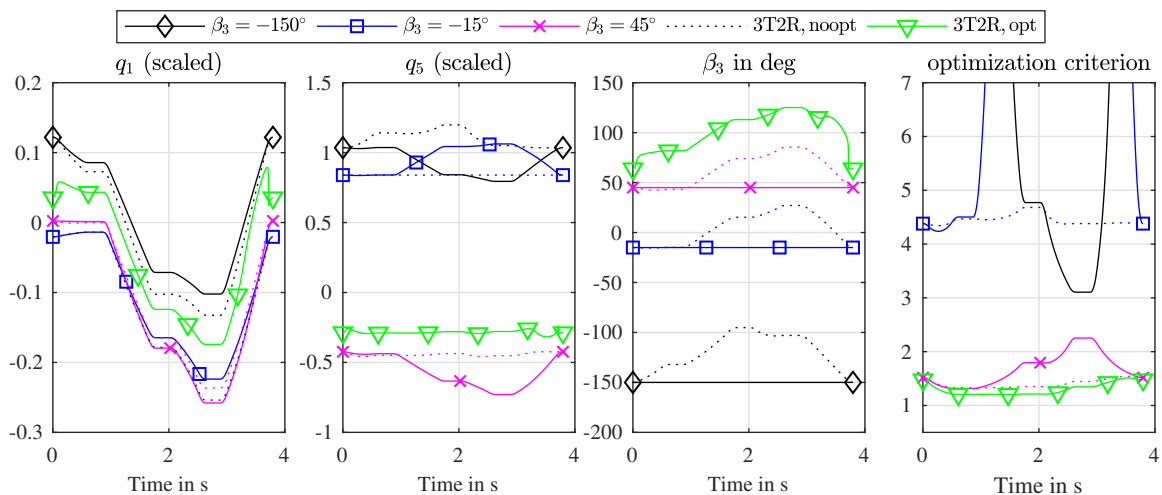


Figure 7. Results of the inverse kinematics with different settings for the trajectory of Fig. 6.

6.2. Resolution of Functional Redundancy of a Parallel Robot in 3T2R tasks

As elaborated in Sec. 4 and 5, the solution of the IKP for 3T2R and 3T3R tasks is necessary to solve the problem for parallel robots. Therefore the trajectory evaluation for a 6UPS parallel robot⁶ in this section is preceded by the trajectory example for a serial link chain in the previous section. This robot belongs to the first class presented in Sec. 1.2, which is primarily addressed in this paper.

The robot has a Gough-structure [15] with symmetric alignment of the universal joint base couplings on a circle with radius $\|r_{0A_i}\| = 1$ m and the spherical joint platform couplings on a circle with radius $\|r_{B_iE}\| = 0.4$ m. The initial pose was set to a center position $x_t^T = [0, 0, 0.5 \text{ m}]$ and the initial orientation x_r was set to zero, meaning an alignment of base and platform frame. The joint positions for each leg were defined to have the initial values $q_i^T = [30^\circ, -30^\circ, 0.583 \text{ m}, 0^\circ, 30^\circ, 60^\circ]$ for the given initial platform pose to avoid switching $\pm\pi$ within the trajectory and to avoid gimbal-lock-singularities. The joint limits were set around the resulting zero position to ± 0.5 m for the prismatic joint and $\pm 60^\circ$ for all single revolute joints representing the universal and spherical joints. The values are higher than typical values for real robots to emphasize the effect of the nullspace movement in a bigger simulated workspace of the robot. The settings for the IK solver are similar as in Sec. 6.1, since both cases regard solving the IKP for a trajectory.

The time evolution of platform pose and optimization criteria is depicted in Fig. 8. The reference trajectory can be seen at the platform position in Fig. 8a and the platform orientation expressed in X-Y-Z-Euler angles (β_1 - β_3) relative to the base frame in Fig. 8b. The IKP is solved using two different methods: Only solving the IKP for the legs separately, called “ser. IK” in Fig. 8 and solving the IKP for all legs together, called “par. IK” in Fig. 8. Both methods perform an optimization with only h_2 of (45), as justified in Sec. 6.1. The first approach only performs this optimization according to Sec. 3 for the first leg using the 3T2R method and then solves the IKP for all other legs with the 3T3R method. The second approach uses the optimization for all legs together according to the 3T2R method from Sec. 4. This results in improved values for the performance criteria depicted for h_1 in Fig. 8c and for h_2 in a logarithmic scale in Fig. 8d. Since the first approach does not regard the limits of the following legs, the optimization criterion gives high values indicating many joint limit violations. The second approach only shows peaks at $t = 1.5$ s in Fig. 8d that result from a joint position getting near to the limit, but not exceeding it. For the practical implementation, the computation time is only weakly influenced by the selection of the method, since calculating the (pseudo)-inverse for six 5×6 and 6×6 or one 35×36 matrices does not present a challenge for current computing hardware. Therefore the “par. IK”-method should be preferred.

⁶ For solving the full IKP, the actuation (such as “6UPS”) does not have to be considered.

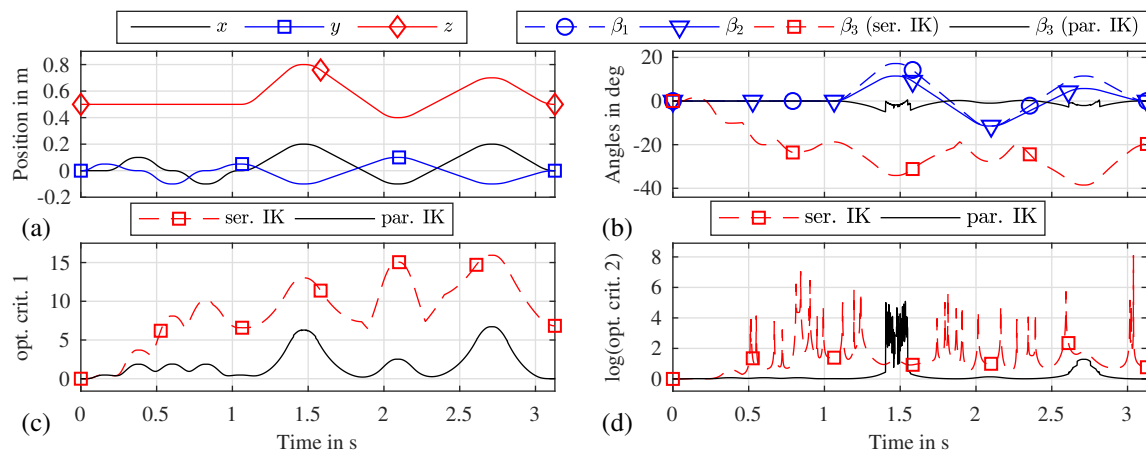


Figure 8. Results of the inverse kinematics of a 6UPS robot in a 3T2R task. (a) platform positions, (b) platform orientation in Euler angles, (c) optimization criterion $h_1(q)$, (d) optimization criterion $h_2(q)$.

6.3. Statistic Results for the Inverse Kinematics of Serial Link Chains

To emphasize the generality of the presented approach, the inverse kinematics is solved for a set of 309 serial kinematic chains with six joints. This set of six-DoF kinematics is generated by permutations of their Denavit-Hartenberg parameters and is reduced with the isomorphism detection of [34] to a minimal set, representing all possible six-DoF serial kinematics with full mobility. The approach is similar to the results of the evolutionary morphology of parallel robot leg chains of [11]. In contrast to the trajectory evaluations in the previous sections focusing on nullspace movement, the inverse kinematics is solved in this section for arbitrary reachable poses of the serial chain in its individual workspace. Therefore, different settings proved to be necessary, since for point-to-point movements, intermediate steps may be outside of the joint limits. In the trajectory case, the initial value for the IKP of the continuous trajectory is always very close to the desired pose of the next trajectory sample. Preventing the algorithm completely from leaving the allowed joint positions reduces the IK success rate. Therefore, the damping term for limit violation was not used in this evaluation, resulting to a constant $K_{\text{Lim}}(q) = 1$ in (47). To reach again an allowed configuration when approaching the goal pose from intermediate steps with limit violations, the combined criterion $h_3(q)$ from (46) with $K_{h1} = 0.99$ and $K_{h2} = 0.01$ was used. Further empirically determined values for all different serial chains were the damping coefficients $K_T = 0.6$ and $K_N = 0.01$ in (47). Since these values provide good results for all serial chains with random geometric parameters and for random configurations, they can be regarded as a good choice generally.

To create a general evaluation case, the poses for testing the IK algorithm were generated by the forward kinematics of 50 different joint configurations of the chains uniformly distributed between the joint limits of $\pm\pi$ for rotational joints and ± 0.5 m for prismatic joints. Additionally, the Denavit Hartenberg parameters were set to 50 different sets of uniformly distributed parameters between 0 and 1 meters or radians resulting to 2500 combinations for each of the 309 chains in total. The initial value q^0 for the solution of the IKP of (47) was set to random values from a uniform distribution within the joint limits. The inverse kinematics was calculated for the full pose with the 3T2R algorithm and only using the pointing direction together with the resolution of functional redundancy in the 3T2R algorithm. A maximum of 15 tries with random initial values was allowed to search for a solution of the IKP within the limits. After that, five more tries were allowed to find a solution violating the limits, but presenting a solution of the IKP to be able to distinguish the two cases, which allows further reasoning on the functionality and possible improvements. A success of the IK is defined as a solution within the joint limits.

The aggregated results are presented as histograms in Fig. 9 for different settings of the algorithm. The histograms show, that for the worst case in 3T2R (3T3R) tasks, the success rate is 87 % (69 %), marked by the position of the first bars in Fig. 9 (a) and (c). These results can be vastly improved by setting the initial guess q^0 within 20 % (w. r. t. the joint limit range) around the pose, from which the desired end-effector pose has been calculated. This improves the worst success rate of all kinematic chains to 98 % for 3T2R (Fig. 9 b) and 95 % for 3T3R tasks (Fig. 9 d).

A detailed investigation on the success rates of all possible serial chains is performed in Fig. 10. The 309 serial kinematics are sorted according to their number of rotational joints and are listed on

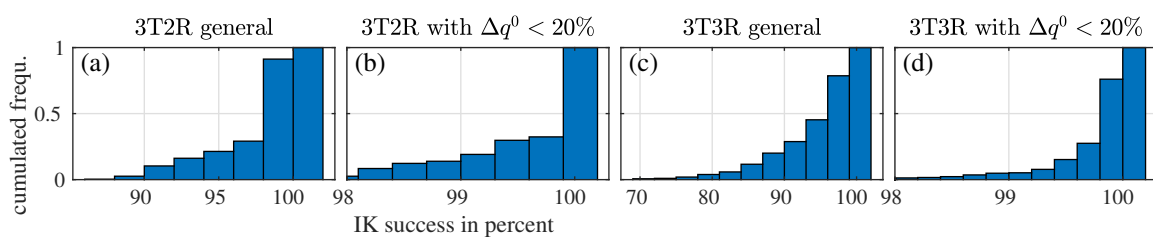


Figure 9. Histograms with cumulated frequency of the IK success for all kinematic chains with different settings: 3T2R tasks (a-b) vs. 3T3R tasks (c-d) and arbitrary initial value (a,c) vs. initial near goal pose.

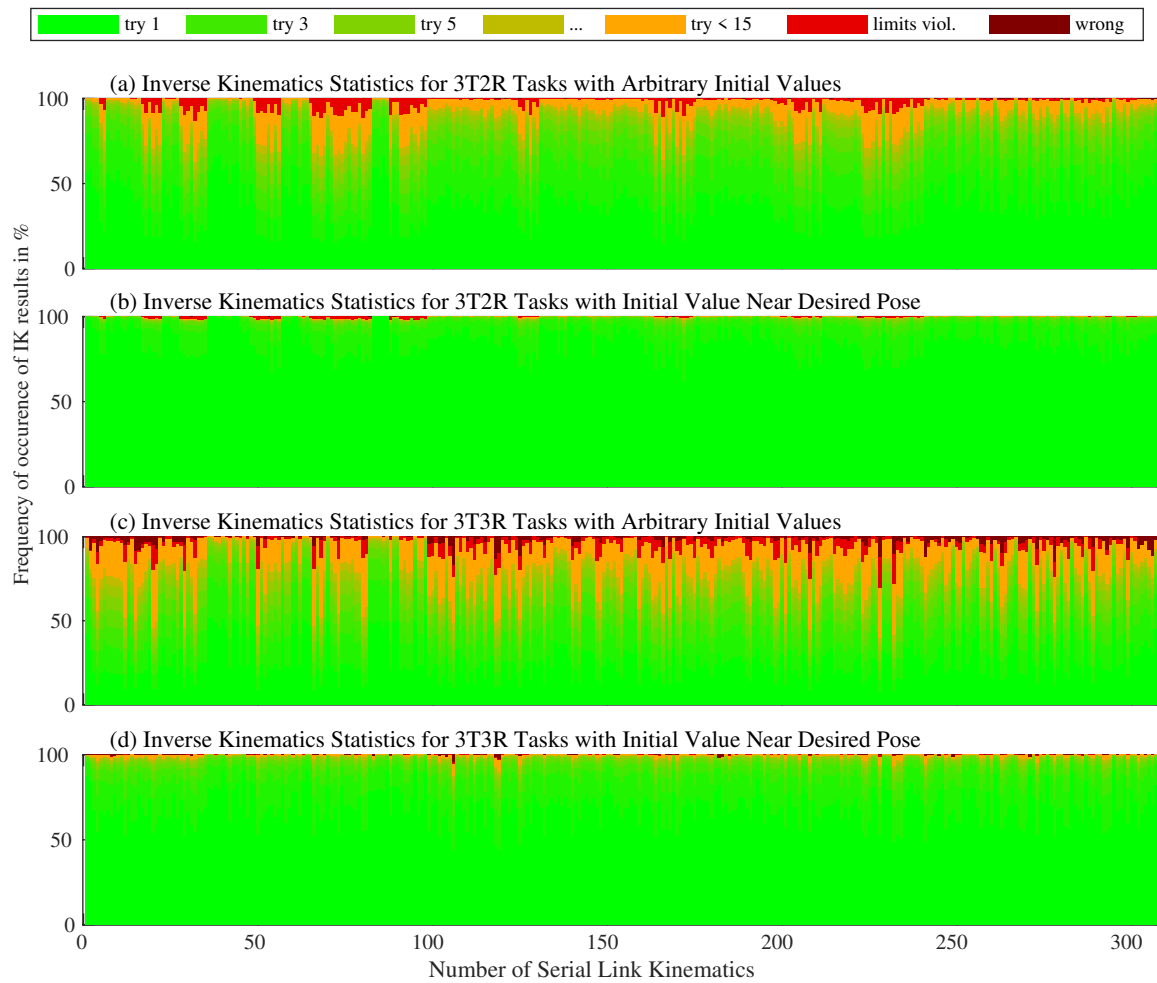


Figure 10. Detailed Statistics of the success of the inverse kinematics algorithm for 3T2R tasks (a-b) and 3T3R tasks (c-d). The Success of the IK solver is shown in different shades of green for increasing numbers of required tries. Different initial values q^0 are distinguished in (a,c) and (b,d).

the horizontal axis of the figure: They contain three rotational joints up to no. 98, four R-joints up to no. 240, and five R-joints up to no. 301. The eight structures from 302 to 309 with six R-joints differ in the parallelism of their joint axes. The first 240 kinematic chains with more than one prismatic joint can be seen as a rather academic example and are listed for the sake of completeness. The most prominent chains are the UPS-chain from Sec. 6.2 at no. 266 and the six-DoF industrial robot from Sec. 6.1 at no. 309. Each bar represents the stacked relative frequency of the IK result state in percent for one kinematic chain. The result state is defined as the number of tries or the success. All bars add up to 100 %, which corresponds to the 2500 configurations per chain. Beginning at the bottom, the number of tries necessary for the solution of the IKP is marked with colors from bright green to orange. Only cases with a violation of the limits (bright red) or wrong position (dark red) correspond to a failure of the algorithm, which has been addressed in the analysis of Fig. 9, representing an aggregated form of Fig. 10. The subfigures (a)-(d) of Fig. 10 correspond to the ones in Fig. 9. It can be observed, that the quality of the results is clustered according to the kinematic groups. Structures with at most one P-joint show a considerably better performance of the algorithm with a worst success rate of 97.16 % for five R-joints and 99.36 % for six R-joints for the 3T2R case (a), which can be seen at the very small red top parts of the bars in the corresponding range of the diagram. The worse performance of the 3T3R algorithm, mostly caused by limit violations, can be explained by joints changing their configuration, i. e. from “elbow up” to “elbow down”, which causes limit violations but does not affect the 3T3R IK.

7. Discussion

A general kinematics model for parallel robots is introduced to solve the inverse kinematics problem for any kind of parallel robot in tasks with one redundant rotational DoF (3T2R). The prize of the generality of the approach is the increased size of the geometric matrices, which is 10×11 for robots with a simple UPS structure instead of 6×6 for the non-redundant kinematics and grow up to 35×36 for general task redundant parallel robots with full mobility. This makes symbolic calculations of the kinematic matrices impossible, allowing only studies on mobility, singularities and other properties of the Jacobian matrix based on numeric calculations. The application of the proposed method can therefore be seen mainly in finding optimal trajectories for task redundant parallel robots in milling or drilling scenarios regarding stiffness, dexterity or joint limits. Due to the performance of the method demonstrated at exemplary cases, an online implementation is possible but has to be proved in future works to converge in real-time conditions for specific machines. The generality of the approach allows to use it in a combined structural and dimensional synthesis sketched in Fig. 2, extending the purely structural synthesis of parallel robot kinematics from [11,31] to a dimensional synthesis of all structures as shown in [34] for serial robots.

Author Contributions: conceptualization, M.S. and S.T.; methodology, M.S.; software, M.S.; validation, M.S.; formal analysis, M.S.; writing—original draft preparation, M.S.; writing—review and editing, M.S., S.T., T.O.; supervision, S.T. and T.O.; project administration, T.O.; funding acquisition, S.T. and T.O.

Funding: The financial support from the Deutsche Forschungsgemeinschaft (German Research Foundation, DFG) under grant number OR 196/33-1 is gracefully acknowledged.

Conflicts of Interest: The authors declare no conflict of interest.

Abbreviations

The following abbreviations are used in this manuscript:

PKM	parallel kinematic machine (parallel robot)
IKP	inverse kinematics problem
DoF	degrees of freedom
$xTyR$	x translational and y rotational degrees of freedom

Appendix A Mathematical Symbols for Reciprocal Euler Angles in Inverse Kinematics

The following appendix contains additional detailed information about the kinematic constraint formulation of this paper. Sec. A.1 contains a mathematical proof for the properties of reciprocal Euler angles in inverse kinematics, which is only outlined in equ. 18 of [5]. The justification for using the approach of partial derivatives instead of the geometric Jacobian is derived in Sec. A.2. The matrix operations for the partial derivatives are replicated from [5] in Sec. A.3 and the contents of the single partial derivatives are given in Sec. A.4 to facilitate the understanding and implementation by the reader.

Appendix A.1 Proof for the Properties of Reciprocal Euler angles

This section derives the effect of the reciprocity of Euler-angles at the example of the kinematics description of Sec. 3 and the frames of Fig. 4 (b): An end-effector orientation $\beta = x_r$ gives the rotation matrix⁷

$${}^D R_E(\beta, q) = {}^0 R_D^T(\beta) {}^0 R_E(q) \quad (A1)$$

⁷ The matrix rotates vectors from \mathcal{F}_E to \mathcal{F}_D

from the actual end-effector frame \mathcal{F}_E to the desired or platform end-effector frame \mathcal{F}_D , where using the X-Y-Z-Euler angles and exploiting the properties of SO(3) rotation matrices yields

$${}^0R_D^T(\beta) = R_z(-\beta_3)R_y(-\beta_2)R_x(-\beta_1) \quad (A2)$$

as introduced in (5). With an additional rotation $-\delta$ around the z-axis for the desired orientation, the resulting new Euler angles β' are

$$\beta'_1 = \beta_1, \quad \beta'_2 = \beta_2, \quad \beta'_3 = \beta_3 - \delta. \quad (A3)$$

The additional rotation corresponds to the tool axis defined in Sec. 3 and leads to a new residual orientation error expressed as a rotation matrix

$$\begin{aligned} {}^D R_E(\beta', q) &= {}^0 R_D^T(\beta') {}^0 R_E(q) \\ &= \left({}^0 R_D(\beta) R_z(-\delta) \right)^T {}^0 R_E(q) \\ &= R_z(\delta) {}^0 R_D^T(\beta) {}^0 R_E(q) \\ &= R_z(\delta) {}^D R_E(\beta, q). \end{aligned} \quad (A4)$$

The first residual orientation error from (A1) corresponding to β is defined as a rotation matrix

$${}^D R_E(\beta, q) = \begin{bmatrix} n_x & o_x & a_x \\ n_y & o_y & a_y \\ n_z & o_z & a_z \end{bmatrix} \quad (A5)$$

and as a Z-Y-X-Euler angle representation⁸

$$\alpha = \begin{bmatrix} \alpha_1 \\ \alpha_2 \\ \alpha_3 \end{bmatrix} = \begin{bmatrix} \arctan2(n_y, n_x) \\ \arctan2(-n_z, \sqrt{a_z^2 + o_z^2}) \\ \arctan2(o_z, a_z) \end{bmatrix}. \quad (A6)$$

The second residual corresponding to β' only differs regarding the additional rotation δ . Combining (A4) and (A5) leads to

$${}^D R_E(\beta', q) = \begin{bmatrix} n'_x & o'_x & a'_x \\ n'_y & o'_y & a'_y \\ n'_z & o'_z & a'_z \end{bmatrix} = \begin{bmatrix} C_\delta n_x - S_\delta n_y & C_\delta o_x - S_\delta o_y & C_\delta a_x - S_\delta a_y \\ C_\delta n_y + S_\delta n_x & C_\delta o_y + S_\delta o_x & C_\delta a_y + S_\delta a_x \\ n_z & o_z & a_z \end{bmatrix},$$

where $C_\delta = \cos(\delta)$ and $S_\delta = \sin(\delta)$. The Z-Y-X-Euler angles from this rotation matrix are

$$\alpha' = \begin{bmatrix} \alpha'_1 \\ \alpha'_2 \\ \alpha'_3 \end{bmatrix} = \begin{bmatrix} \arctan2(n'_y, n'_x) \\ \arctan2(-n'_z, \sqrt{a'^2_z + o'^2_z}) \\ \arctan2(o'_z, a'_z) \end{bmatrix} = \begin{bmatrix} \arctan2((C_\delta n_y + S_\delta n_x), (C_\delta n_x - S_\delta n_y)) \\ \arctan2(-n_z, \sqrt{a_z^2 + o_z^2}) \\ \arctan2(o_z, a_z) \end{bmatrix}, \quad (A7)$$

⁸ Utilizing the sign-aware operator $\arctan2(y, x)$ instead of $\arctan(y/x)$ allows angles to be in $(-\pi, +\pi]$, removes ambiguities and provides global differentiability.

where δ only influences the first component α'_1 . This allows the conclusion, that β_3 only influences α_1 and results in the dependencies

$$\alpha'_1 = \alpha'_1(\mathbf{q}, \beta_1, \beta_2, \beta_3) \quad (\text{A8})$$

$$\alpha'_2 = \alpha'_2(\mathbf{q}, \beta_1, \beta_2) = \alpha_2 \quad (\text{A9})$$

$$\alpha'_3 = \alpha'_3(\mathbf{q}, \beta_1, \beta_2) = \alpha_3 \quad (\text{A10})$$

395 with the consequences for the kinematic modeling of robots in 3T2R tasks described in Sec. 3.

396 Appendix A.2 Relation of the Gradient Matrices to the Geometric Jacobian of the Serial Chain

As introduced in Sec. 5, the rotational part of the gradient matrices can not be derived with the commonly available Jacobian of the serial link kinematics of the legs. Defining the residual of the orientation for the inverse kinematics with Euler angles was first introduced in [7], where the calculation of the partial derivatives was referred to the geometric Jacobian without further clarification. The relationship between the gradient matrices from Sec. 5 and the Jacobian can be obtained by comparing the platform or end-effector velocity

$$\dot{\mathbf{x}} = J_1 \dot{\mathbf{q}}_1, \quad \begin{bmatrix} \dot{\mathbf{x}}_t \\ \dot{\mathbf{x}}_r \end{bmatrix} = \begin{bmatrix} J_{t,1}(\mathbf{q}_1) \\ J_{r,1}(\mathbf{q}_1) \end{bmatrix} \dot{\mathbf{q}}_1 \quad (\text{A11})$$

obtained with the Jacobian with the velocity obtained by the gradient matrices of (18). Using the differential form (29) only for the first kinematic leg chain of the parallel robot gives

$$\frac{d}{dt} \Phi_1(\mathbf{q}_1, \mathbf{x}) = \Phi_{1,q}(\mathbf{q}_1, \mathbf{x}) \dot{\mathbf{q}}_1 + \Phi_{1,x}(\mathbf{q}_1, \mathbf{x}) \dot{\mathbf{x}} = \mathbf{0} \quad (\text{A12})$$

and results reorganized to the form of (A11) with (32) and (35) to

$$\begin{bmatrix} \dot{\mathbf{x}}_t \\ \dot{\mathbf{x}}_r \end{bmatrix} = - \begin{bmatrix} -\mathbf{1} & \mathbf{0} \\ \mathbf{0} & \Phi_{r,1,\partial x_r}^{-1} \end{bmatrix} \begin{bmatrix} \Phi_{t,1,\partial q_1} & \Phi_{r,1,\partial q_1} \end{bmatrix} \dot{\mathbf{q}}_1 = \begin{bmatrix} \Phi_{t,1,\partial q_1} & \mathbf{0} \\ \mathbf{0} & -\Phi_{r,1,\partial x_r}^{-1} \Phi_{r,1,\partial q_1} \end{bmatrix} \dot{\mathbf{q}}_1. \quad (\text{A13})$$

By equating coefficients of (A11) and (A13) the relations

$$\Phi_{1,q}(\mathbf{q}_1) = -\Phi_{1,x}(\mathbf{q}_1, \mathbf{x}) J_1(\mathbf{q}_1), \quad (\text{A14})$$

$$\Phi_{t,1,\partial q_1}(\mathbf{q}_1) = J_{t,1}(\mathbf{q}_1) \quad \text{and} \quad (\text{A15})$$

$$\Phi_{r,1,\partial q_1}(\mathbf{q}_1, \mathbf{x}) = -\Phi_{r,1,\partial x_r}(\mathbf{q}_1, \mathbf{x}) J_{r,1}(\mathbf{q}_1) \quad (\text{A16})$$

397 can be obtained between the gradient matrices and the analytic Jacobian of the serial leg chain. The
 398 dependency on \mathbf{q}_1 and \mathbf{x} has been added to highlight the main requirement, namely the zero equality
 399 condition of (A12). In the inverse kinematics procedure of Sec. 5.3 the residual at step k in (40) is
 400 unequal to zero. For the partial derivative (36)/I a value of ${}^D\overline{\mathbf{R}}_E \neq \mathbf{1}$ will be inserted in (A20), which
 401 will break (A16). The translational part is unaffected, as can be seen in (A15).

402 Appendix A.3 Matrix Operations for Partial Derivatives

To simplify the calculations of the gradient matrices of the residuals in Sec. 5, operators for matrices are replaced by operators for vectors, to avoid differentiating matrices or w.r.t. matrices which

would require multi-dimensional tensors. The column operator \bar{R} for rotation matrices R to stack the coordinate systems unit vectors $n, o, a \in \mathbb{R}^3$ vertically instead of horizontally is defined as

$$\bar{R}(R) = \begin{bmatrix} n \\ o \\ a \end{bmatrix} \in \mathbb{R}^9 \quad \text{with} \quad R = \begin{bmatrix} n & o & a \end{bmatrix} = \begin{bmatrix} n_x & o_x & a_x \\ n_y & o_y & a_y \\ n_z & o_z & a_z \end{bmatrix} \in \text{SO}(3) \quad (\text{A17})$$

to avoid differentiating matrices or w.r.t. matrices. The special properties of the $\text{SO}(3)$ group are not exploited and the operator can be used for $\mathbb{R}^{3 \times 3}$ as well. Matrix multiplication is expressed with the matrix product operator $\bar{\Pi}$ such that

$${}^1\bar{R}_3 = \bar{\Pi}({}^1\bar{R}_2, {}^2\bar{R}_3) = \bar{R}({}^1R_3) \quad \text{with} \quad {}^1R_3 = {}^1R_2 {}^2R_3. \quad (\text{A18})$$

The transposition operator P_T is a 9×9 permutation matrix such that

$${}^2\bar{R}_1 = P_T {}^1\bar{R}_2 = \bar{R}({}^1R_2^T) = {}^1\bar{R}_2^T \in \mathbb{R}^9 \quad \text{with} \quad {}^2R_1 = {}^1R_2^T \in \text{SO}(3) \quad \text{and} \quad {}^1\bar{R}_2 = \bar{R}({}^1R_2). \quad (\text{A19})$$

403 Writing ${}^1\bar{R}_2^T$ instead of $P_T {}^1\bar{R}_2$ serves for the clarity of the expressions (34,36,38,39) and overloads the
404 transposition operator for \mathbb{R}^9 noted with the bar.

405 Appendix A.4 Contents of the Partial Derivatives

The single expressions derived in Sec.5 can be calculated with low computational effort from the definition of the X-Y-Z- and Z-Y-X-Euler angles from (5), (21) and (A6). With $\bar{R} = [n_x, n_y, n_z, o_x, o_y, o_z, a_x, a_y, a_z]^T$ the gradient “I” in (34,36,38,39) for Z-Y-X angles becomes

$$\frac{\partial \alpha(\bar{R})}{\partial \bar{R}} = \begin{bmatrix} -\frac{n_y}{n_x^2 + n_y^2} & \frac{n_x}{n_x^2 + n_y^2} & 0 & 0 & 0 & 0 & 0 & 0 & 0 \\ 0 & 0 & -\sqrt{a_z^2 + o_z^2} & 0 & 0 & \frac{n_z o_z}{\sqrt{a_z^2 + o_z^2}} & 0 & 0 & \frac{n_z a_z}{\sqrt{a_z^2 + o_z^2}} \\ 0 & 0 & 0 & 0 & 0 & \frac{a_z}{a_z^2 + o_z^2} & 0 & 0 & -\frac{o_z}{a_z^2 + o_z^2} \end{bmatrix} \quad (\text{A20})$$

and the inverse gradient “IV” in (36) for X-Y-Z angles yields

$$\frac{\partial \bar{R}(\beta)}{\partial \beta} = \begin{bmatrix} 0 & -S_2 C_3 & -C_2 S_3 \\ C_1 S_2 C_3 - S_1 S_3 & S_1 C_2 C_3 & -S_1 S_2 S_3 + C_1 C_3 \\ S_1 S_2 C_3 + C_1 S_3 & -C_1 C_2 C_3 & C_1 S_2 S_3 + S_1 C_3 \\ 0 & S_2 S_3 & -C_2 C_3 \\ -C_1 S_2 S_3 - S_1 C_3 & -S_1 C_2 S_3 & -S_1 S_2 C_3 - C_1 S_3 \\ -S_1 S_2 S_3 + C_1 C_3 & C_1 C_2 S_3 & C_1 S_2 C_3 - S_1 S_3 \\ 0 & C_2 & 0 \\ -C_1 C_2 & S_1 S_2 & 0 \\ -S_1 C_2 & -C_1 S_2 & 0 \end{bmatrix} \quad (\text{A21})$$

with $C_i = \cos(\beta_i)$, $S_i = \sin(\beta_i)$. The property

$$\left(\frac{\partial \beta}{\partial \bar{R}} \right) \left(\frac{\partial \bar{R}(\beta)}{\partial \beta} \right) = \mathbf{1} \in \mathbb{R}^{3 \times 3} \quad (\text{A22})$$

can be used to test the implementation, if (A20, A21) are defined for the same Euler-angle notation. The gradient of the matrix product (A18) w.r.t. the second factor used in (34)/II, (36)/III, (38)/II and (39)/III is

$$\frac{\partial}{\partial \bar{\mathbf{R}}_2} \bar{\Pi}(\bar{\mathbf{R}}_1, \bar{\mathbf{R}}_2) = \begin{bmatrix} \mathbf{R}_1 & \mathbf{0} & \mathbf{0} \\ \mathbf{0} & \mathbf{R}_1 & \mathbf{0} \\ \mathbf{0} & \mathbf{0} & \mathbf{R}_1 \end{bmatrix} \quad (\text{A23})$$

and to complete the enumeration the gradient w.r.t. the first factor is

$$\frac{\partial}{\partial \bar{\mathbf{R}}_1} \bar{\Pi}(\bar{\mathbf{R}}_1, \bar{\mathbf{R}}_2) = \begin{bmatrix} \text{diag}(n_x) & \text{diag}(o_x) & \text{diag}(a_x) \\ \text{diag}(n_y) & \text{diag}(o_y) & \text{diag}(a_y) \\ \text{diag}(n_z) & \text{diag}(o_z) & \text{diag}(a_z) \end{bmatrix}, \quad (\text{A24})$$

where n_x, n_y, \dots are the entries of \mathbf{R}_2 and the diag-matrices are 3×3 . By transposing the elements of the matrix product (A18), only the first form (A23) had to be used in this paper.

References

- Baron, L. A joint-limits avoidance strategy for arc-welding robots. *Int. Conf. on Integrated Design and Manufacturing in Mech. Eng.* 2000, pp. 16–19.
- Huo, L.; Baron, L. Kinematic inversion of functionally-redundant serial manipulators: application to arc-welding. *Transactions of the Canadian Society for Mechanical Engineering* **2005**, *29*, 679–690. doi:10.1139/tcsme-2005-0045.
- Léger, J.; Angeles, J. Off-line programming of six-axis robots for optimum five-dimensional tasks. *Mechanism and Machine Theory* **2016**, *100*, 155–169. doi:10.1016/j.mechmachtheory.2016.01.015.
- Žlajpah, L. On orientation control of functional redundant robots. *IEEE International Conference on Robotics and Automation (ICRA)*, 2017, pp. 2475–2482. doi:10.1109/ICRA.2017.7989288.
- Schappeler, M.; Tappe, S.; Ortmaier, T. Resolution of Functional Redundancy for 3T2R Robot Tasks using Two Sets of Reciprocal Euler Angles. *Proc. of the 15th IFToMM World Congress*, 2019. Accepted for publication. Preliminary Download Link: <https://dl.uni-h.de/?t=6685463677171c469502082ce750ee06>, doi:10.1007/978-3-030-20131-9_168.
- Yoshikawa, T. Analysis and control of robot manipulators with redundancy. *Robotics research: the first international symposium*. MIT press Cambridge, MA, 1984, pp. 735–747.
- Goldenberg, A.; Benhabib, B.; Fenton, R. A complete generalized solution to the inverse kinematics of robots. *IEEE Journal on Robotics and Automation* **1985**, *1*, 14–20. doi:10.1109/JRA.1985.1086995.
- Zhu, W.; Qu, W.; Cao, L.; Yang, D.; Ke, Y. An off-line programming system for robotic drilling in aerospace manufacturing. *The International Journal of Advanced Manufacturing Technology* **2013**, *68*, 2535–2545. doi:10.1007/s00170-013-4873-5.
- Guo, Y.; Dong, H.; Ke, Y. Stiffness-oriented posture optimization in robotic machining applications. *Robotics and Computer-Integrated Manufacturing (RCIM)* **2015**, *27*, 367–376. doi:10.1016/j.rcim.2015.02.006.
- Tale-Masouleh, M.; Gosselin, C. Singularity analysis of 5-RPUR parallel mechanisms (3T2R). *The International Journal of Advanced Manufacturing Technology* **2011**, *57*, 1107–1121. doi:10.1007/s00170-011-3349-8.
- Gogu, G. *Structural Synthesis of Parallel Robots, Part 1: Methodology*; Vol. 866, *Solid Mechanics and Its Applications*, Springer, 2008.
- Huang, T.; Liu, H.; Chetwynd, D. Generalized Jacobian analysis of lower mobility manipulators. *Mechanism and Machine Theory* **2011**, *46*, 831–844. doi:10.1016/j.mechmachtheory.2011.01.009.
- Merlet, J.P.; Perng, M.W.; Daney, D. Optimal trajectory planning of a 5-axis machine-tool based on a 6-axis parallel manipulator. In *Advances in Robot Kinematics*; Springer, 2000; pp. 315–322. doi:10.1007/978-94-011-4120-8_33.
- Hong, K.S.; Kim, J.G. Manipulability analysis of a parallel machine tool: application to optimal link length design. *Journal of robotic Systems* **2000**, *17*, 403–415.

15. Merlet, J.P. *Parallel Robots*, 2nd ed.; Vol. 128, *Solid Mechanics and Its Applications*, Springer Science & Business Media, 2006.
16. Zhang, D. *Parallel robotic machine tools*; Springer Science & Business Media, 2009.
17. Wang, J.; Gosselin, C.M. Kinematic analysis and singularity representation of spatial five-degree-of-freedom parallel mechanisms. *Journal of Robotic Systems* **1997**, *14*, 851–869. doi:10.1002/(SICI)1097-4563(199712)14:12<851::AID-ROB3>3.0.CO;2-T.
18. Zhang, D.; Gosselin, C.M. Kinetostatic modeling of N-DOF parallel mechanisms with a passive constraining leg and prismatic actuators. *Journal of Mechanical Design* **2001**, *123*, 375–381. doi:10.1115/1.1370976.
19. Zheng, K.J.; Gao, J.S.; Zhao, Y.S. Path control algorithms of a novel 5-DOF parallel machine tool. IEEE International Conference on Mechatronics and Automation, 2005, Vol. 3, pp. 1381–1385. doi:10.1109/ICMA.2005.1626755.
20. Gao, J.S.; Sun, H.; Zhao, Y.S. The primary calibration research of a measuring limb in 5-UPS/PRPU parallel machine tool. IEEE International Conference on Intelligent Mechatronics and Automation, 2004, pp. 304–308. doi:10.1109/ICIMA.2004.1384209.
21. Liu, X.; Xu, Y.; Yao, J.; Xu, J.; Wen, S.; Zhao, Y. Control-faced dynamics with deformation compatibility for a 5-DOF active over-constrained spatial parallel manipulator 6PUS–UPU. *Mechatronics* **2015**, *30*, 107–115. doi:10.1016/j.mechatronics.2015.06.014.
22. Wen, S.; Qin, G.; Zhang, B.; Lam, H.K.; Zhao, Y.; Wang, H. The study of model predictive control algorithm based on the force/position control scheme of the 5-DOF redundant actuation parallel robot. *Robotics and Autonomous Systems* **2016**, *79*, 12–25. doi:10.1016/j.robot.2016.02.002.
23. Mbarek, T.; Nefzi, M.; Corves, B. Prototypische Entwicklung und Konstruktion eines neuartigen Parallelmanipulators mit dem Freiheitsgrad fünf. *VDI-Berichte* **2005**. In German. Further information: <https://www.igmr.rwth-aachen.de/index.php/en/rob-en/rob-pentapod-en>; accessed June 20th 2019.
24. Schreiber, H.; Gosselin, C. Analyse et conception d'un manipulateur parallèle spatial à cinq degrés de liberté. *Mechanism and machine theory* **2003**, *38*, 535–548. doi:10.1016/S0094-114X(03)00007-7.
25. Gao, F.; Peng, B.; Zhao, H.; Li, W. A novel 5-DOF fully parallel kinematic machine tool. *The International Journal of Advanced Manufacturing Technology* **2006**, *31*, 201. doi:10.1007/s00170-005-0171-1.
26. Bär, G.F.; Weiß, G. Kinematic Analysis of a Pentapod Robot. *Journal for Geometry and Graphics* **2006**.
27. Lin, W.; Li, B.; Yang, X.; Zhang, D. Modelling and control of inverse dynamics for a 5-DOF parallel kinematic polishing machine. *International Journal of Advanced Robotic Systems* **2013**, *10*, 314. doi:10.5772/54966.
28. Alagheband, A.; Mahmoodi, M.; Mills, J.K.; Benhabib, B. Comparative analysis of a redundant pentapod parallel kinematic machine. *Journal of Mechanisms and Robotics* **2015**, *7*, 034502. doi:10.1115/1.4028933.
29. Gogu, G. Fully-isotropic parallel manipulators with five degrees of freedom. IEEE International Conference on Robotics and Automation, 2006, pp. 1141–1146. doi:10.1109/ROBOT.2006.1641863.
30. Huang, Z.; Li, Q.C. General Methodology for Type Synthesis of Symmetrical Lower-Mobility Parallel Manipulators and Several Novel Manipulators **2002**. *21*, 131–145. doi:10.1177/027836402760475342.
31. Kong, X.; Gosselin, C.M. Type synthesis of 5-DOF parallel manipulators based on screw theory. *Journal of Robotic Systems* **2005**, *22*, 535–547. doi:10.1002/rob.20084.
32. Tale-Masouleh, M.; Saadatzi, M.H.; Gosselin, C.; Taghirad, H.D. A geometric constructive approach for the workspace analysis of symmetrical 5-PRUR parallel mechanisms (3T2R). ASME International Design Engineering Technical Conferences and Computers and Information in Engineering Conference, 2010, pp. 1335–1344. doi:10.1115/DETC2010-28509.
33. Cheng, L.; Wang, H.; Zhao, Y. Analysis and experimental investigation of parallel machine tool with redundant actuation. International Conference on Intelligent Robotics and Applications. Springer, 2008, pp. 179–188. doi:10.1007/978-3-540-88513-9_20.
34. Ramirez, D.; Kotlarski, J.; Ortmaier, T. Automatic generation of a minimal set of serial mechanisms for a combined structural - geometrical synthesis. Proc. of the 14th IFToMM World Congress; , 2015. doi:10.6567/IFTToMM.14TH.WC.OS13.047.
35. Briot, S.; Khalil, W. *Dynamics of Parallel Robots*; Springer, 2015.
36. Huo, L.; Baron, L. The joint-limits and singularity avoidance in robotic welding. *Industrial Robot: An International Journal* **2008**, *35*, 456–464. doi:10.1108/01439910810893626.